Supplementary Information

Superacidity in Zr(IV)/Ce(III) MOF-808: unlocking biodiesel production from microalgae lipids at reduced temperatures

Lei Qian[1], Jun Cheng[2,1*], Kai Xin[1], Yuxiang Mao[1], Jiacan Tu[3]， Weijuan Yang[1]

1 State Key Laboratory of Clean Energy Utilization, Zhejiang University, Hangzhou 310027, China

2 Key Laboratory of Low-grade Energy Utilization Technologies and Systems of Ministry of Education, Chongqing University, Chongqing 400044, China

[*] Corresponding author: Prof. Dr. Jun Cheng, State Key Laboratory of Clean Energy Utilization, Zhejiang University, Hangzhou 310027, China. Tel.: +86 571 87952889; fax: +86 571 87951616. E-mail: juncheng@zju.edu.cn

Content

Section S1 Syntheses of the Catalysts

1.1 Materials

The marine microalgae *Nannochloropsis oceanica* were provided by Yantai Hearol Biotechnology Co., Ltd. (Shandong, China). Zirconium oxychloride octahydrate (99.9%, $ZrOCl_2 \cdot 8H_2O$), cerium(III) chloride heptahydrate (99%, $CeCl_3 \cdot 7H_2O$), and benzene-1,3,5-tricarboxylic acid (99%, H_3BTC) were purchased from Macklin Biochemical Co., Ltd. (Shanghai, China). N,N-dimethyl formamide (99%, DMF), formic acid (99%), methanol (99.9%), chloroform (99%), sulfuric acid (96%), 2,4-dinitrofluorobenzene (99%), trimethylphosphine oxide (97%, TMPO), deuterated dimethyl sulfoxide (99%, DMSO-d6), and hydrofluoric acid (48 wt% aqueous solution) and *n*-hexane (98%) were obtained from Aladdin Industrial Inc. (Shanghai, China). Methanol-d (CH_3OD, 99.5 Atom % D) was obtained from Sigma. All starting materials and solvents, unless otherwise specified, were used without further purification.

1.2 Analytical techniques.

Unless otherwise specified, all samples were subjected to vacuum drying at 150 °C prior to the test. X-ray diffraction (XRD) was conducted on an X'Pert^3 PRO diffractometer (Malvern Panalytical, UK, the Netherlands) operated at 40 kV with Cu Kα radiation using a scanning speed of 2^o min^{-1}. Scanning electron microscopy (SEM) and energy-dispersive X-ray spectroscopy (EDS) were performed on an Oxford Xplore 50 instrument (ZEISS Sigma 300) equipped with an EDS system. Nitrogen absorption-desorption experiments were performed with a Quantachrome Autosorb-iQ3 instrument (Micromeritics, USA) at -196 °C to determine Brunauer–Emmett–Teller (BET) surface areas and pore size distributions. The yield and composition of fatty acid methyl esters were analyzed using a gas chromatograph (Agilent 7890A, USA). Solution 1H NMR spectra were acquired on a Bruker Avance III HD 400MHz NMR spectrometer. Trace elemental analysis of carbon and hydrogen (EA) was conducted using a Perkin Elmer 2400 elemental analyzer. Inductively coupled plasma optical emission spectroscopy (ICP-OES) was performed using a PerkinElmer Optima 5300 DV instrument. Thermogravimetric analysis coupled with mass spectrometry (TG-MS) was conducted using the Thermo Plus EVO_2/ Thermo Mass Photo instrument (Thermo Fisher Scientific, USA). High-resolution solid-state nuclear magnetic

resonance (NMR) spectra were recorded at ambient temperature using a standard Agilent Magic Angle Spinning (MAS) probe with a 4 mm (outer diameter) zirconia rotor on an Agilent DSX-300 spectrometer.

1.3 General procedure for sample preparation.

All glassware used for handling the MOF samples was dried under vacuum at 130 °C for 3 hours and subsequently cooled to room temperature before immediate use. After synthesis, the MOF was washed with DMF to remove any residual unreacted ions on the surface. The washed MOF was then immersed in 150 ml of methanol to remove any remaining DMF and activate the catalyst. Subsequently, the methanol-exchanged sample was dried under vacuum at 50°C for 24 hours to obtain the dried sample. Unless otherwise specified, all catalysts were treated in a vacuum oven at 150°C for 24 hours prior to use.

The molecular formula of the MOF was determined using a combination of elemental analysis (C, H), ^{1}H NMR (ratio of BTC to formate and methanol), ICP-OES (Zr, Ce), and TGA-MS. A mixture containing 300 μL of DMSO-d6 and 300 μL of hydrofluoric acid (48 wt% aqueous solution) was used to digest 10 mg of each MOF sample for subsequent ^{1}H NMR measurements. Samples were subjected to microwave-assisted digestion, conducted at 500 W and 100°C for 30 minutes to enhance efficiency. After digestion, the containers were allowed to cool to room temperature, and the digestion solution was filtered to remove any residues. Finally, the digested samples were subjected to ^{1}H NMR measurements.

1.4 Synthesis of catalysts

MOF-808.

The synthesis of the pristine MOF-808 was prepared using a slightly modified published procedure[1]. Typically, 9 mmol of $ZrOCl_2 \cdot 8H_2O$ (2.9 g) and 3 mmol of H_3BTC (0.63 g) were dissolved in 300 ml of DMF/formic acid (150 mL/150 mL) and stirred at room temperature until a clear solution was obtained. The solution containing the dissolved linker (H_3BTC) and metal ions (Zr(IV)) was transferred to a 500 ml Teflon-lined autoclaves and heated to 120°C for 3 days. The white precipitate was collected by centrifugation and washed 3 times with 150 ml of fresh DMF. Subsequently, the synthesized MOF-808 was immersed in 150 ml anhydrous methanol for three

days, with three consecutive methanol exchanges each day. After the methanol exchange process, the compound was filtered, evacuated at room temperature for 24 hours, and then subjected to vacuum at 150°C for another 24 hours to generate activated samples.

^{1}H solution NMR spectrum of the digested and activated MOF-808 (400 MHz, DMSO-*d6*): 8.64 (s, BTC), 8.12 (s, HCOOH), and 3.57 (s, CH_3OH). Molar ratio (BTC: HCOOH: CH_3OH)= 2:5.3:0.03. Anal calcd for $[Zr_6O_4(OH)_4(C_9H_3O_6)_2(HCOO)_{5.3}](H_2O)_{1.4}$= $Zr_6C_{23.3}H_{18.1}O_{32}$： Zr, 40.34%; C, 20.6%, O, 37.73%; H, 1.33%. Found: Zr, 40.59%; C, 20.34%, O, 37.78%; H, 1.29%.

Zr(IV)/Ce(III) Bimetallic MOF-808

Bimetallic Zr/Ce-MOF-808 was prepared in a similar manner to that of the pristine MOF-808 by the one-pot method. A series of bimetallic Zr/Ce-MOF-808s were obtained by adjusting the molar ratio of the two metal ions, Zr(IV) and Ce(III), while ensuring a total ion number of 9 mmol (Table s1). For example, Zr(IV) 6 mmol/ Ce(III) 3mol， Zr(IV) 4.5 mmol/ Ce(III) 4.5mol and Zr(IV) 3 mmol/ Ce(III) 6mol, and labelled as Zr/Ce(2:1)-MOF-808, Zr/Ce(1:1)-MOF-808, Zr/Ce(1:2)-MOF-808.

^{1}H solution NMR spectrum of the digested and activated Zr/Ce(2:1)-MOF-808 (400 MHz, DMSO-*d6*): 8.64 (s, BTC), 8.12 (s, HCOOH), and 3.57 (s, CH_3OH). Molar ratio (BTC: HCOOH: CH_3OH)=2:4.8:2.3. Anal calcd for $[Zr_{3.94}Ce_{2.06}O_4(OH)_4(C_9H_3O_6)_2(HCOO)_{4.8}](CH_3OH)_{2.3}(H_2O)_{0.1}$= $Zr_{3.94}Ce_{2.06}C_{25.1}H_{24.2}O_{32}$： Zr, 24.20%; Ce, 19.43%; C, 20.28%, O, 34.46%; H, 1.63%. Found: Zr, 24.17%; Ce, 19.41%; C, 20.14%, O, 34.60%; H, 1.68%

^{1}H solution NMR spectrum of the digested and activated Zr/Ce(1:1)-MOF-808 (400 MHz, DMSO-*d6*): 8.64 (s, BTC), 8.12 (s, HCOOH), and 3.57 (s, CH_3OH). Molar ratio (BTC: HCOOH: CH_3OH)= 2:4.3:3.1. Anal calcd for $[Zr_{3.55}Ce_{2.45}O_4(OH)_4(C_9H_3O_6)_2(HCOO)_{4.3}](CH_3OH)_{3.1}(H_2O)_{0.3}$= $Zr_{3.55}Ce_{2.45}C_{25.4}H_{27.3}O_{32}$： Zr, 21.43%; Ce, 22.72%; C, 20.17%, O, 33.88%; H, 1.81%. Found: Zr, 21.35%; Ce, 22.63%; C, 20.22%, O, 33.94%; H, 1.86%

Ce(III)-MOF-808 （for comparative purposes only）

9 mmol of $CeCl_3 \cdot 7H_2O$ (3.35 g) and 3 mmol of H_3BTC (0.63 g) were dissolved in 300 ml of DMF/formic acid (150 mL/150 mL) and stirred at room temperature until a clear solution was

obtained. The solution containing the dissolved linker (H_3BTC) and metal ions (Ce(III)) was transferred to a 500 ml Teflon-lined autoclaves and heated to 120°C for 3 days. The precipitate was collected by centrifugation and washed 2 times with 150 ml of fresh DMF. Then, the catalysts were activated by methanol exchange and dried.

Table S1 Synthesis of catalysts

Catalyst	$ZrCl_2O·8H_2O$		$CeCl_3·7H_2O$		H_3BTC	DMF	Formic acid
MOF-808	9 mmol	2.9 g	0 mmol	0 g	3 mmol 0.63 g	150 ml	150 ml
Zr/Ce(2:1)-MOF-808	6 mmol	1.93 g	3 mmol	1.12 g			
Zr/Ce(1:1)-MOF-808	4.5 mmol	1.45 g	4.5 mmol	1.68 g			
Zr/Ce(1:2)-MOF-808	3 mmol	0.97 g	6 mmol	2.24 g			
Ce(III)-MOF-808	0 mmol	0 g	9 mmol	3.35 g			

Table S2 Porosity properties of various catalysts

Catalyst	S_{BET} ($m^2g·cat^{-1}$)	Average pore size (nm)	Pore volume ($cm^3g·cat^{-1}$)	
			Total (V_p)	Micropore (V_{micro})
MOF-808	1125	1.64	0.494	0.354
Zr/Ce (2:1)-MOF-808	1790	1.71	0.766	0.578
Zr/Ce (1:1)-MOF-808	1912	1.76	0.782	0.566
Zr/Ce (1:2)-MOF-808	1044	1.77	0.514	0.308
Ce(III)-MOF-808	9.92	5.39	0.014	0.01

Section S2 Powder X-ray Diffraction Patterns

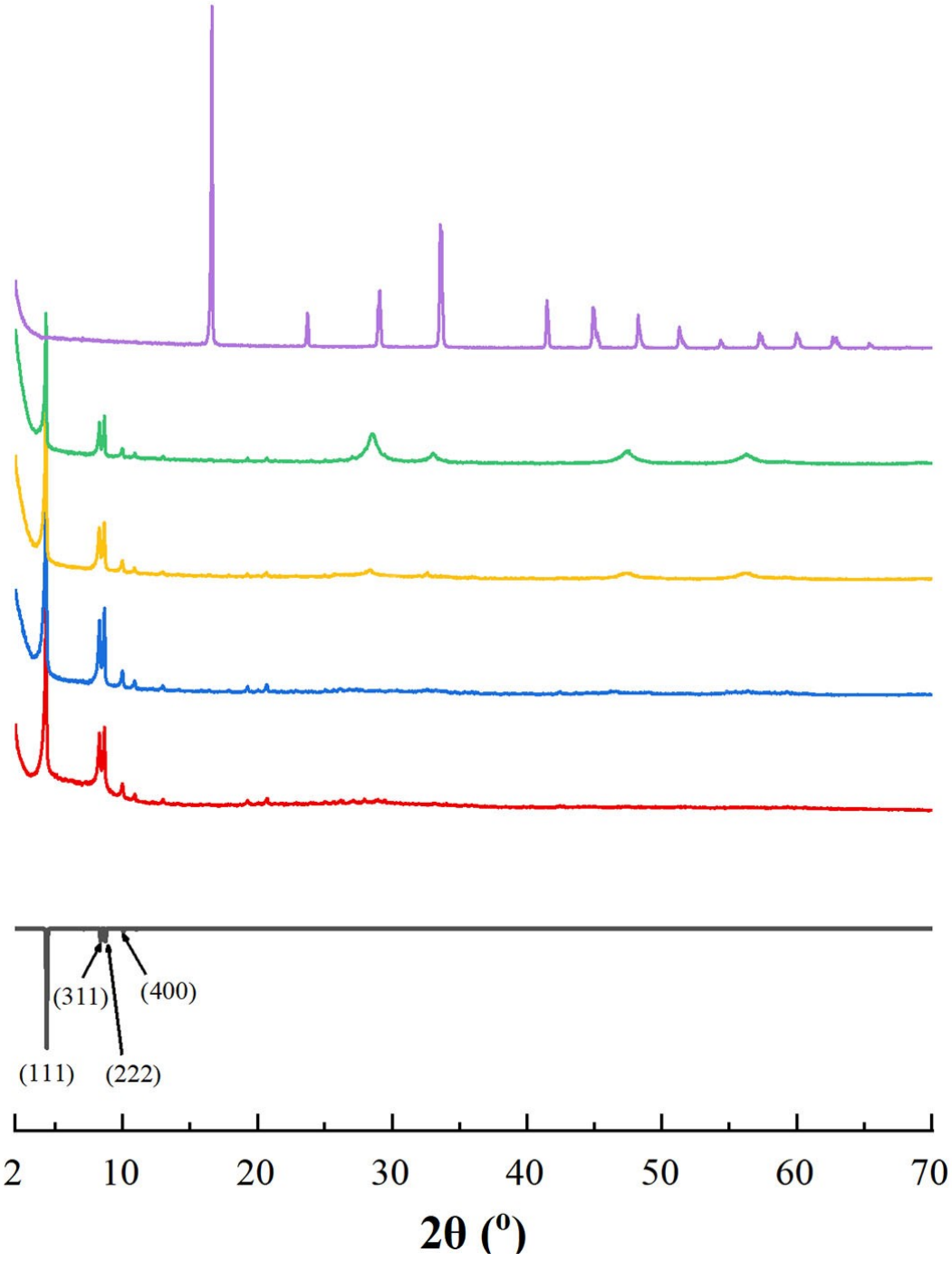

Fig. S1. Experimental XRD patterns of MOF-808 (red), Zr/Ce(2:1)-MOF-808 (blue), Zr/Ce(1:1)-MOF-808 (yellow), Zr/Ce(1:2)-MOF-808 (green), Ce(III)-MOF-808 (purple) and simulated pattern (black) from MOF-808 (Section S1).

Section S3 SEM and EDS

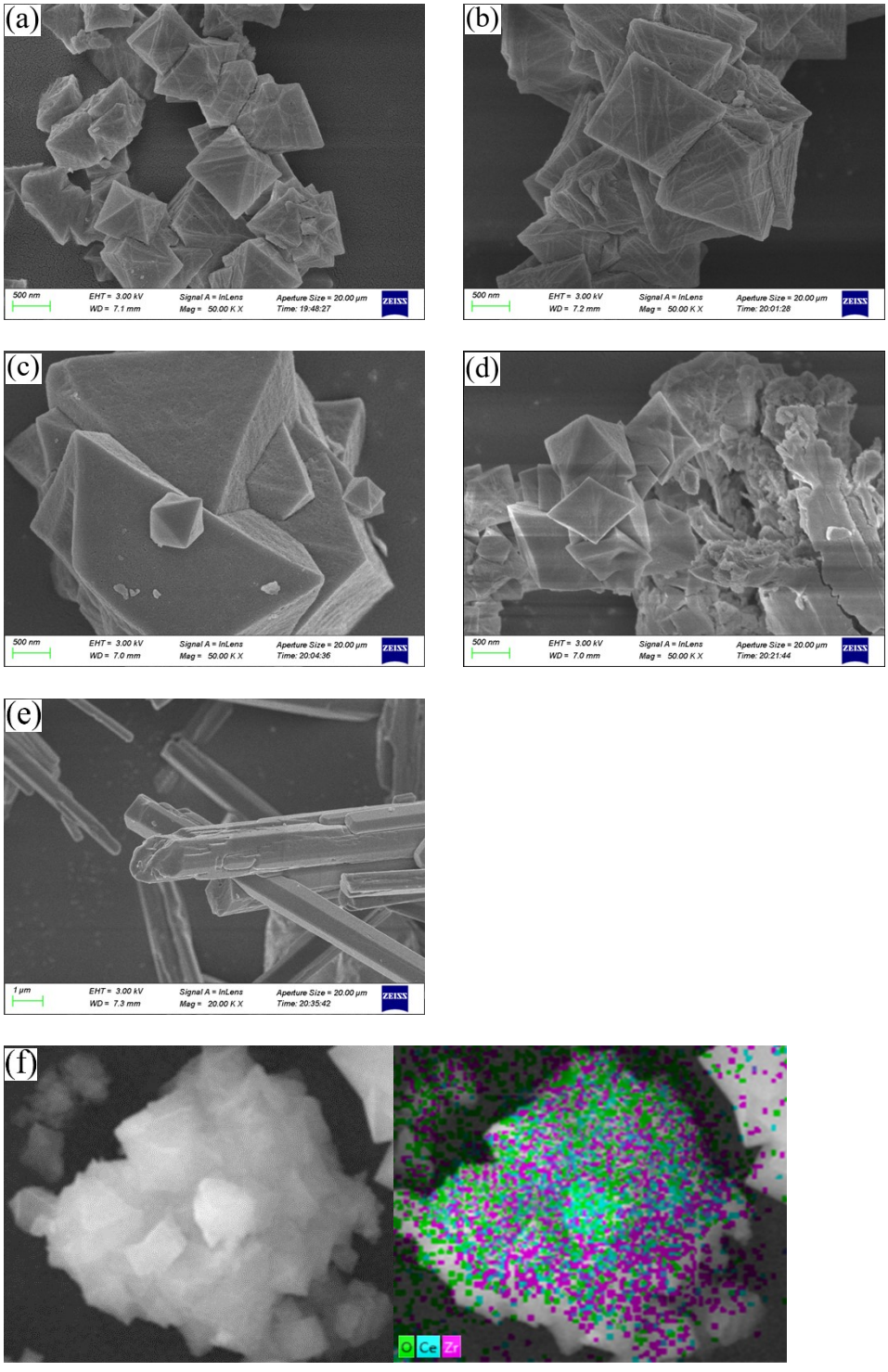

Fig. S2. SEM images of (a) MOF-808 (b) Zr/Ce(2:1)-MOF-808 (c) Zr/Ce(1:1)-MOF-808 (d) Zr/Ce(1:2)-MOF-808 (e) Ce(III)-MOF-808 (f) EDS images of Zr/Ce(1:1)-MOF-808

Section S4 Thermogravimetric analysis coupled with mass spectrometry

The synthesized catalyst underwent examination employing thermogravimetric analysis coupled with mass spectrometry (TG-MS) to derive its thermogravimetric profile and scrutinize the gas composition released during the temperature ramp-up process. Briefly, a 6 mg sample was weighed in a reaction tube and purged under a helium gas flow (40 mL min-1), heated to 200 °C for drying and pretreatment, then cooled to 50 °C, and finally heated to 800 °C at a rate of 10 °C min-1, and the changes in mass and pyrolysis gas was analyzed.

The obtained thermogravimetric curve provided insights into the catalyst's thermal stability and decomposition profile, while the analysis of the evolved gases allowed for the identification and quantification of different gas species released during the thermal decomposition process.

Fig. S3 depicts the TG-MS analysis results of MOF-808 and Zr/Ce(1:1)-MOF-808. It is evident that within the 200-400°C temperature range, the predominant thermal decomposition gas of MOF-808 is H_2O. This is attributed to the presence of residual water resulting from the partial replacement of formic acid sites during the synthesis process. Conversely, Zr/Ce(1:1)-MOF-808 exhibits a gas composition of CO, CO_2, H_2 and H_2O during decomposition, indicating the presence of methanol (as an activator) occupying the formic acid sites, as confirmed by the ^1H solution NMR spectrum (Supplementary Section S1).

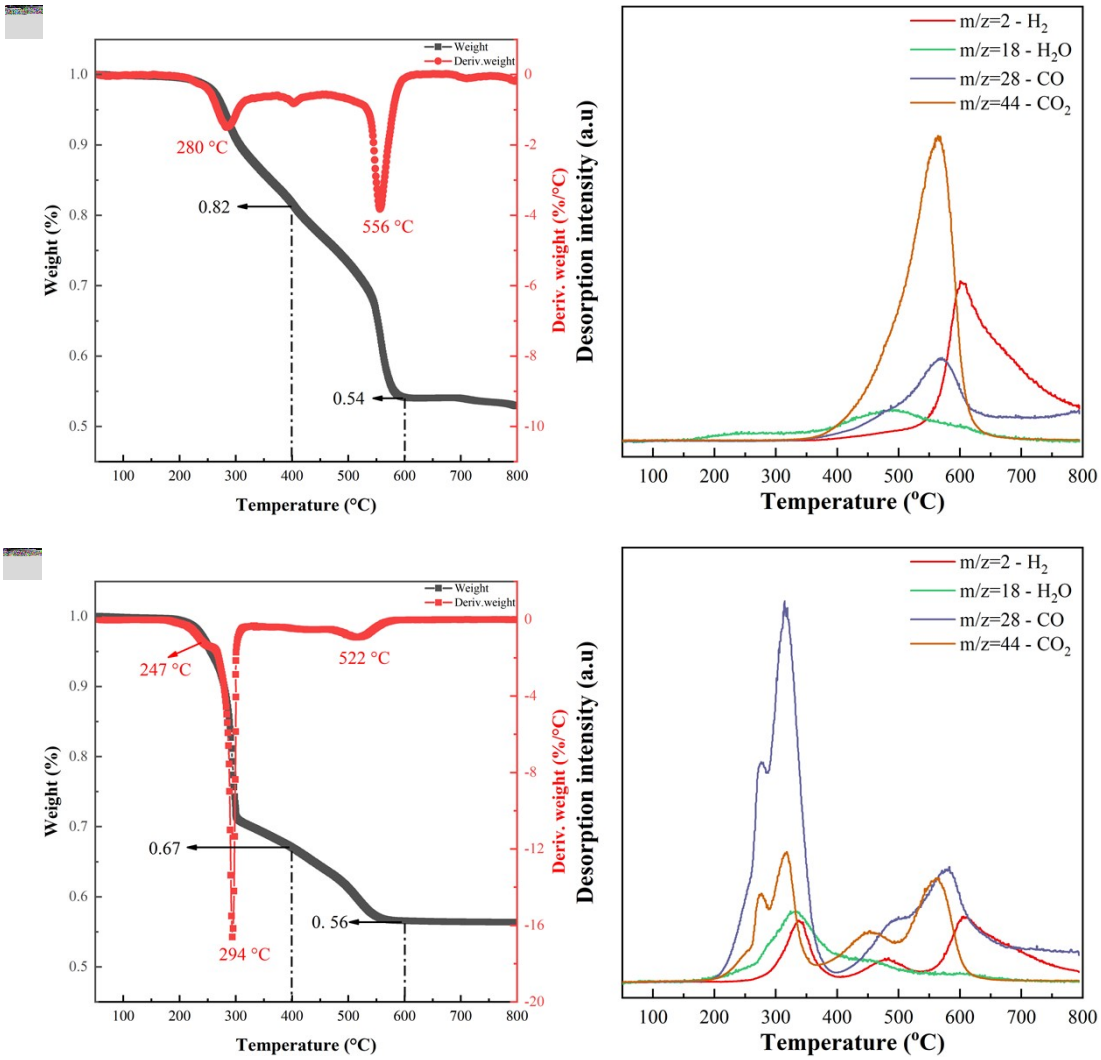

Fig. S3 TG-MS analysis of (a) MOF-808, (b) Zr/Ce(1:1)-MOF-808

Section S5 Solid-state ^{31}P NMR

Sample preparation: The preparation of ^{31}P solid-state nuclear magnetic resonance (SSNMR) samples was conducted with slight modifications based on previously reported procedures [1]. Approximately 100 mg of each MOF sample was activated and placed into a 1.5 mL chloroform solution of 0.2 M trimethylphosphine oxide (TMPO) and thoroughly mixed within an inert atmosphere glovebox. The resulting suspension was vacuum evacuated overnight at room temperature under dynamic vacuum and subsequently subjected to vacuum treatment at 50°C for 8 hours. The sample was then transferred under an argon atmosphere into 4 mm (outer diameter) ZrO_2 NMR sample rotors equipped with airtight caps.

Experimental parameters: The solid-state ^{31}P MAS NMR spectra were acquired on an Agilent 600 DD2 spectrometer operating at a resonance frequency of 242.77 MHz for ^{31}P nuclei. The experiment employed magic angle spinning (MAS) and high-power 1H decoupling techniques to enhance the resolution and spectral quality of SSNMR experiments. A ^{31}P signal from a 0 ppm aqueous solution (85%) of H_3PO_3 served as an external reference for chemical shift calibration. Spectra were obtained using a spinning rate of 10 kHz (90° pulse of 4.2 μs) and a recycle delay of 3 s.

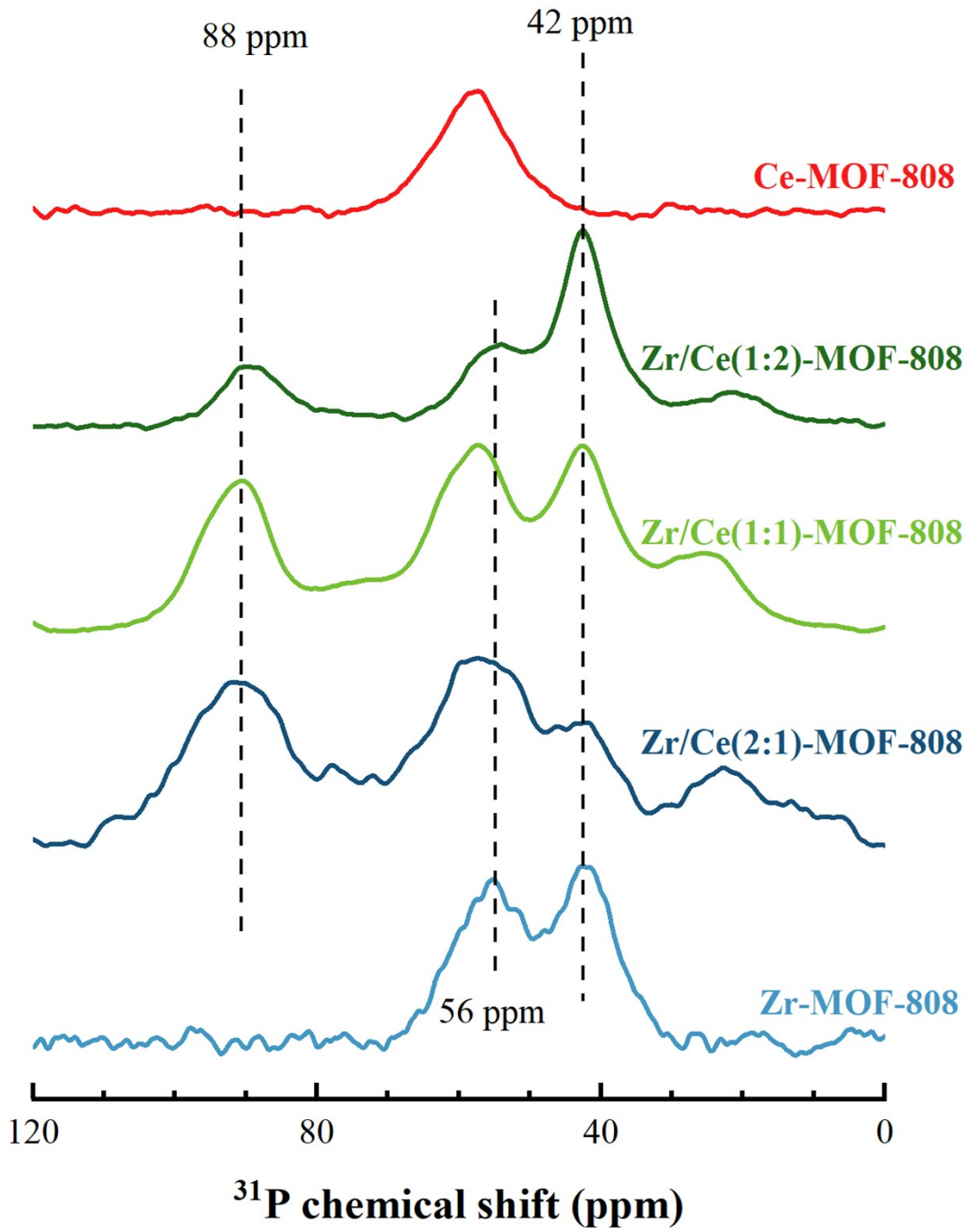

Fig. S4 ^{31}P SSNMR spectra of MOF-808, Zr/Ce(1:2)-MOF-808, Zr/Ce(1:1)-MOF-808, Zr/Ce(1:2)-MOF-808 and Ce-MOF-808

Section S6 Solid-state ^{1}H NMR

Sample preparation: The preparation of ^{1}H SSNMR samples involves treatment with deuterated methanol (CH_3OD) and methanol (CH_3OH). In brief, approximately 100 mg of each MOF sample were subjected to treatment at 150°C in a vacuum oven for 24 hours. Subsequently, these samples were placed in 3 ml of CH_3OD or CH_3OH solutions and thoroughly mixed within an inert atmosphere glovebox. The resulting suspensions were vacuum-evacuated overnight at room temperature under dynamic vacuum, followed by 8 hours of vacuum treatment at 50°C. The samples were then transferred under an argon atmosphere into 4 mm (outer diameter) ZrO_2 NMR sample rotors equipped with airtight caps.

Experimental parameters: The solid-state ^{1}H MAS NMR spectra were acquired on an Agilent 600 DD2 spectrometer (magnetic field strength 14.1 T) operating at a ^{1}H resonance frequency of 599.72 MHz. The ^{1}H chemical shifts were referenced externally to tetramethylsilane (TMS) at 0 ppm. The experiment utilized MAS to enhance the resolution and spectral quality of the SSNMR experiments. Spectra were obtained using a spinning rate of 10 kHz (90° pulse of 4.2 μs) and a recycle delay of 3 s.

Section S7 Variable-temperature infrared spectroscopy (VTIR)

Sample preparation: The preparation of VTIR samples involved a methanol treatment process. Initially, approximately 10 mg of each MOF sample underwent a 24-hour treatment at 150°C in a vacuum oven. Post-treatment, these samples were immersed in 3 ml methanol solutions and thoroughly mixed within an inert atmosphere glovebox. The resulting suspensions were subjected to overnight vacuum evacuation at room temperature under dynamic vacuum, followed by an additional 8-hour vacuum treatment at 50°C. Subsequently, 2 mg of MOF powder sample was uniformly ground with 200 mg of pure KBr in an argon atmosphere, placed into a mold, and compressed into transparent films using a hydraulic press. Finally, these samples were transferred to the FTIR spectrometer measurement chamber, pre-washed with argon gas.

Experimental parameters: VTIR was performed using a Thermo iS10 spectrometer. The sample underwent activation in an argon atmosphere at 50°C until spectral stability was attained. Infrared spectra were recorded in the wavenumber range of 550-4000 cm^{-1} with 32 scans and a resolution of 4 cm^{-1}. In the range of 50-200°C, the sample was scanned after maintaining a constant temperature at intervals of 10°C for 5 minutes, with a heating rate of 2°C/min.

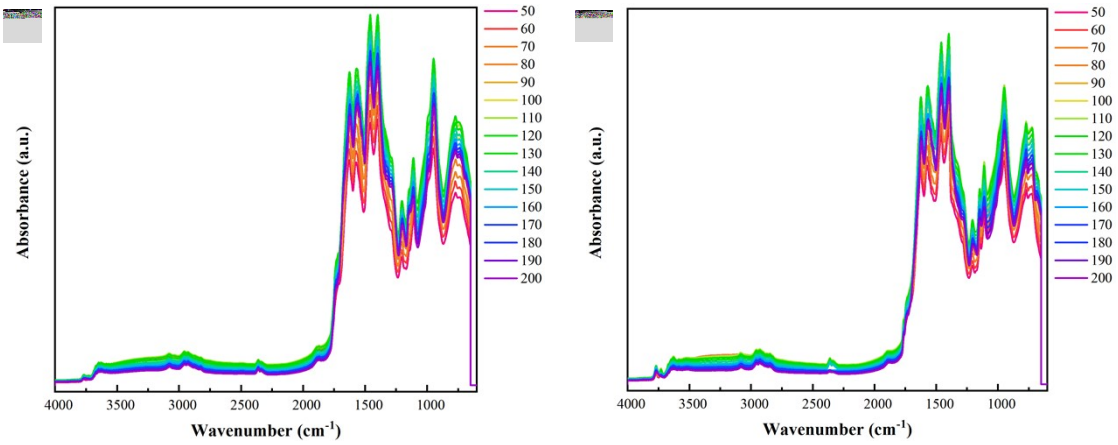

Fig. S5 VTIR spectra of (a) MOF-808 and (b) Zr/Ce(1:1)-MOF-808

Section S8 Density functional theory (DFT) calculation

The initial structure of MOF-808 was obtained from the CCDC database (https://www.ccdc.cam.ac.uk/), specifically from the structure published by Christopher et al. [2] (MOF-808 CCDC 1871192).

8.1 Optimization of the lattice structure of MOF-808

Based on the structural formula $Zr_6O_4(OH)_4(BTC)_2(HCOO)_6$, geometric optimization of the MOF-808 unit cell was performed under the convergence conditions of Max. force 0.002 Ha/Å and Max. displacement of 0.005 Å. The structural optimization of MOF-808 was conducted under three-dimensional periodic boundary conditions, allowing relaxation of atomic positions and lattice parameters. The Generalized Gradient Approximation (GGA) was employed using the Perdew-Burke-Ernzerhof (PBE) exchange-correlation functional to approximate the gradient of the electron density, characterizing the electronic interactions within the system. DFT Semi-core Pseudopts were chosen to handle core electrons and nuclei, reducing computational complexity while ensuring higher accuracy. The DNP basis set was used to model the distribution of valence electrons [3]. To account for charge transfer and delocalization effects, Grimme's dispersion correction (D3) was included in each calculation[4,5]. The convergence criteria for each atom during the self-consistent field calculations were set at 2.0e-6 Ha, with a maximum of 100 convergence cycles and an orbital cutoff of 5.2 Å. To accelerate convergence and stabilize iterations, a smearing value of 0.005 Ha and a DIIS size of 6 were applied, along with the utilization of a charge density preconditioner to expedite convergence, set at 10 a_0^{-1}, considering the significant number of atoms within the MOF system.

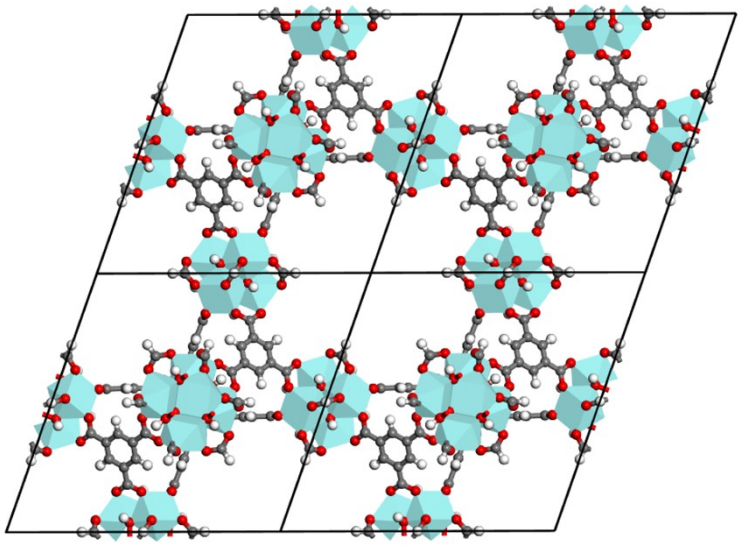

Fig. S6 Schematic representation of the unit cell structure of MOF-808.

The crystal structure exhibits m-3m space group symmetry, which corresponds to a cubic symmetry with a face-centered cubic lattice. The unit cell lattice parameters were initially a = b = c = 24.845 Å, α = β = γ = 60°, and after optimization, the lattice parameters became a = b = c = 25.113 Å, α = β = γ = 60°.

8.2 Cluster structure optimization

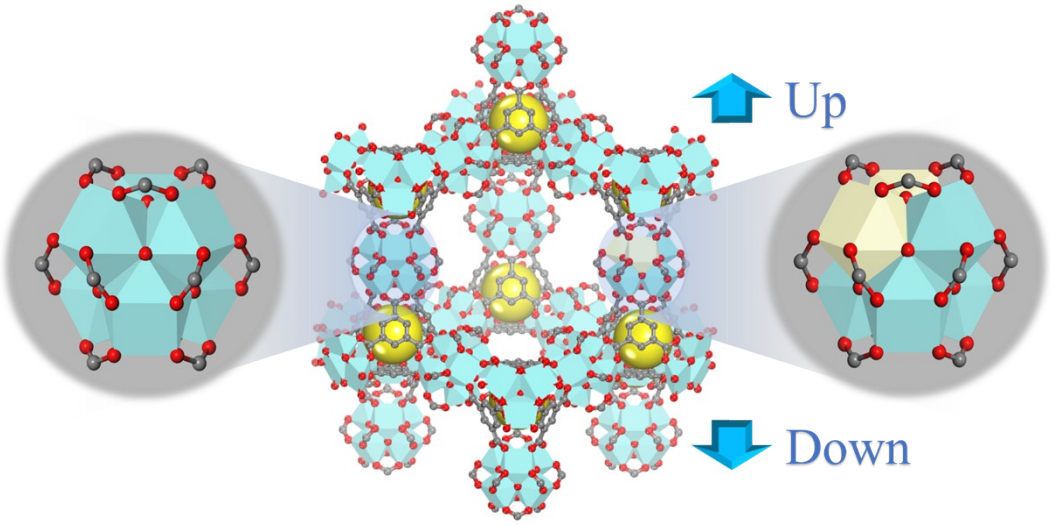

Fig. S7 Directional schematic of cluster structure

XRD test results indicate that the introduction of Ce atoms had small impact on the catalyst lattice structure (Fig. S1). Considering the computational load, an optimized simplified method based on Christopher et al.'s work was adopted [2]. Acetate groups replaced BTC as terminal ligands, and the coordinates of the C atoms in the methyl groups were fixed, resulting in the structure $Zr_6O_4(OH)_4(C_2H_3O_2)_6(COOH)_6$. GGA-PBE was used to describe the electronic interactions within the system. DFT semi-core pseudopotentials were applied to handle the core electrons and atomic nuclei. The DNP basis set was employed to model the valence electron distribution [3]. To address charge transfer and delocalization effects effectively, Grimme dispersion correction (D3) [4,5] was included in each computation. The convergence criterion for each atom in the self-consistent field calculation was set to 2.0e-6 Ha, with a maximum convergence limit of 100 iterations. The orbital cutoff was established at 5.2 Å. Tail corrections were implemented with a smearing value of 0.005 Ha, using a DIIS size of 6 to accelerate iteration and ensure convergence stability. Due to the higher atom count in the MOF system, a charge density preconditioner was employed to expedite convergence.

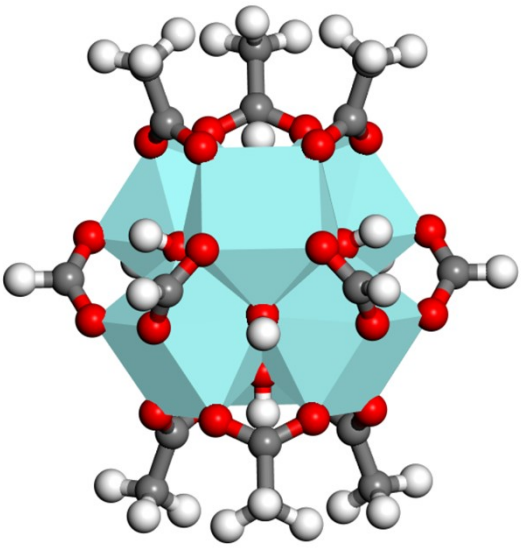

Fig. S8 Diagram of the optimized structure of the cluster

8.3 Doping energy

Doping energy refers to the energy change caused by the introduction of dopant atoms into a structure. It arises due to alterations in the lattice and electronic band structures resulting from the

presence of these dopant atoms. A lower doping energy value signifies a more favorable reaction and increased stability of the doped structure. As Ce atoms in MOF-808 are solely doped within the cluster structure, utilizing the optimized cluster structure enables exploration of configurations with the lowest doping energy when varying Ce atom proportions. In the symmetrical distribution of six equivalent Zr atoms within the cluster structure, Ce atoms maintain symmetry in their substitution positions. As illustrated in the Fig. S9, with the incorporation of one Ce atom, the SBU configuration remains singular, denoted as Zr_5Ce_1. When incorporating two Ce atoms, there are three SBU configurations labeled as Zr_4Ce_2-a, Zr_4Ce_2-b, Zr_4Ce_2-c. For three Ce atom inclusions, three distinct configurations are observed, noted asZr_3Ce_3-a, Zr_3Ce_3-b, Zr_3Ce_3-c. The configurations of four and five Ce atom inclusions are derived by substituting Zr atoms with Ce atoms from the Zr_4Ce_2-a, Zr_4Ce_2-b, Zr_4Ce_2-c, Zr_5Ce_1 configurations and vice versa, designated as Zr_2Ce_4-a, Zr_2Ce_4-b, Zr_2Ce_4-c, Zr_1Ce_5.

The doping energy of different configurations in Zr/Ce-MOF-808 can be calculated using the following formula:

$$\Delta E_{dope} = E_{Zr_{6-n}{}^{SBU}Ce_n} + E_{Zr_n} - \left(E^{SBU}_{Zr_6} + E_{Ce_n}\right)$$

Here, ΔE_{dope} represents the doping energy; $E_{Zr_{6-n}{}^{SBU}Ce_n}$ denotes the total energy of the cluster structure consisting of 6-n Zr atoms and n Ce atoms in the SBU; E_{Zr_n} represents the total energy of n Zr atoms; $E^{SBU}_{Zr_6}$ indicates the total energy of the cluster structure composed of 6 Zr atoms in the SBU; E_{Ce_n} signifies the total energy of n Ce atoms

It should be noted that the structural optimization of the doping model may lead to non-convergence of SCF. This is primarily due to the much larger radius of Ce atoms compared to Zr atoms, leading to the possibility of significant atomic distance elongation or distortion and the presence of small minima during the structural optimization process. Properly increasing the smearing value and electron density mixing parameters helps accelerate SCF convergence and mitigate oscillations and instability in calculations. On the other hand, the application of Grimme D3 correction [4] is employed to account for dispersion interactions.

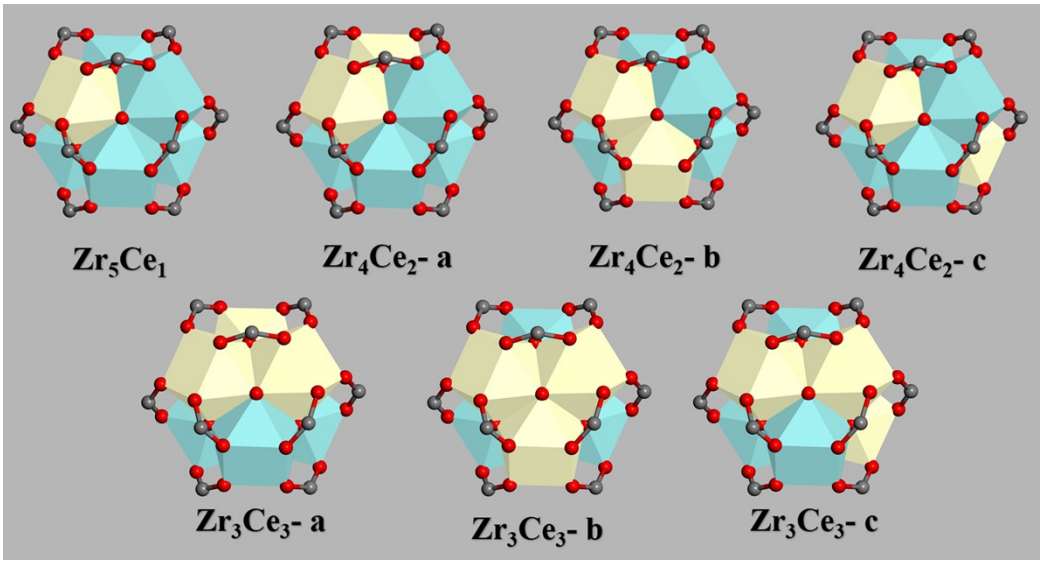

Fig. S9 The schematic diagrams of various doping configurations

8.4 The calculation of adsorption energies for different surface configurations and Crystal Orbital Hamilton Population (COHP).

We further investigated the adsorption modes of methanol on cluster surfaces and proton distribution by selecting the Zr_4Ce_2-c configuration with the lowest doping energy (-8.81 kJ/mol). Considering the loss of formic acid and the substitution of methanol in the catalyst, we represented the average clusters in the modeling process by the molecular formula $Zr_4Ce_2O_4(OH)_4(C_2H_3O_2)_6(COOH)_x(CH_3OH)_y$, where x = 5 or 6; y = 1 or 2. The optimized configurations are shown in Table 1 and are named using the cluster structure name (Zr_4Ce_2) + the quantities of formic acid and methanol (x = 5 or 6; y = 1 or 2) + the form of methanol adsorption (Top/Hollow/Bridge) + a numerical identifier, such as Zr_4Ce_2-Perfect-Top-a.

Adsorption energy is a measure of the ability of molecules or atoms to adsorb on the surface or within the pores of a solid, influenced by various factors of interaction between substances such as van der Waals forces, electrostatic interactions, hydrogen bonds, and chemical bonds, among others. The adsorption energy (E_{ads}) can be calculated using the following formula:

$$E_{ads} = E_{total} - E_{Cat.} - E_{MeOH}$$

Here, E_{ads} represents the adsorption energy, E_{total} is the total energy of the system after the catalyst adsorbs methanol, $E_{Cat.}$ is the ground-state energy of the catalyst, and E_{MeOH} is the total

energy of the methanol molecule. Adsorption energy indicates the strength of interaction between the adsorbate molecules and the catalyst surface, where negative values denote stable adsorption and positive values indicate stable desorption.

COHP is a commonly used method in the study of solid-state electronic structures, employed to analyze the chemical bonding properties between atoms within solids. COHP computations are based on DFT, utilizing the Hamiltonian describing the interaction between band structures and atomic orbitals obtained from DFT calculations to elucidate the strength and nature of chemical bonds.

COHP can be calculated using the following formula:

$$COHP(E) = -\frac{1}{\pi}\int DOS(E) \cdot IP_{DOS(E)} dE$$

Where COHP(E) represents the value of COHP at energy E. DOS(E) stands for the total Density of States of the crystal, indicating the number of electrons at energy E. $IP_{DOS(E)}$ refers to the Integrated Projected Density of States, describing the interaction between specific pairs of atomic orbitals at energy E.

8.5 Model Zr_4Ce_2-x5y2-Top's Mulliken Population Analysis (MPA) for and Density of States (DOS) analysis

The electron transfer and orbital overlap were confirmed by Mulliken population analysis (MPA) and density of states (DOS) analysis of the model Zr_4Ce_2-x5y2-Top before and after the reaction (Fig. S10). So, the respective reaction can be described as the acquisition of electrons by the hydroxyl group in methanol from the Ce atom, weakening the stability of the C-O bond, while the disturbed methyl group overcoming the energy barrier moves away from the hydroxyl group, breaking the C-O bond and approaching the Ce atom. This process involves electron rearrangement between the p-orbitals of the C atom and the d and s orbitals of the Ce atom.

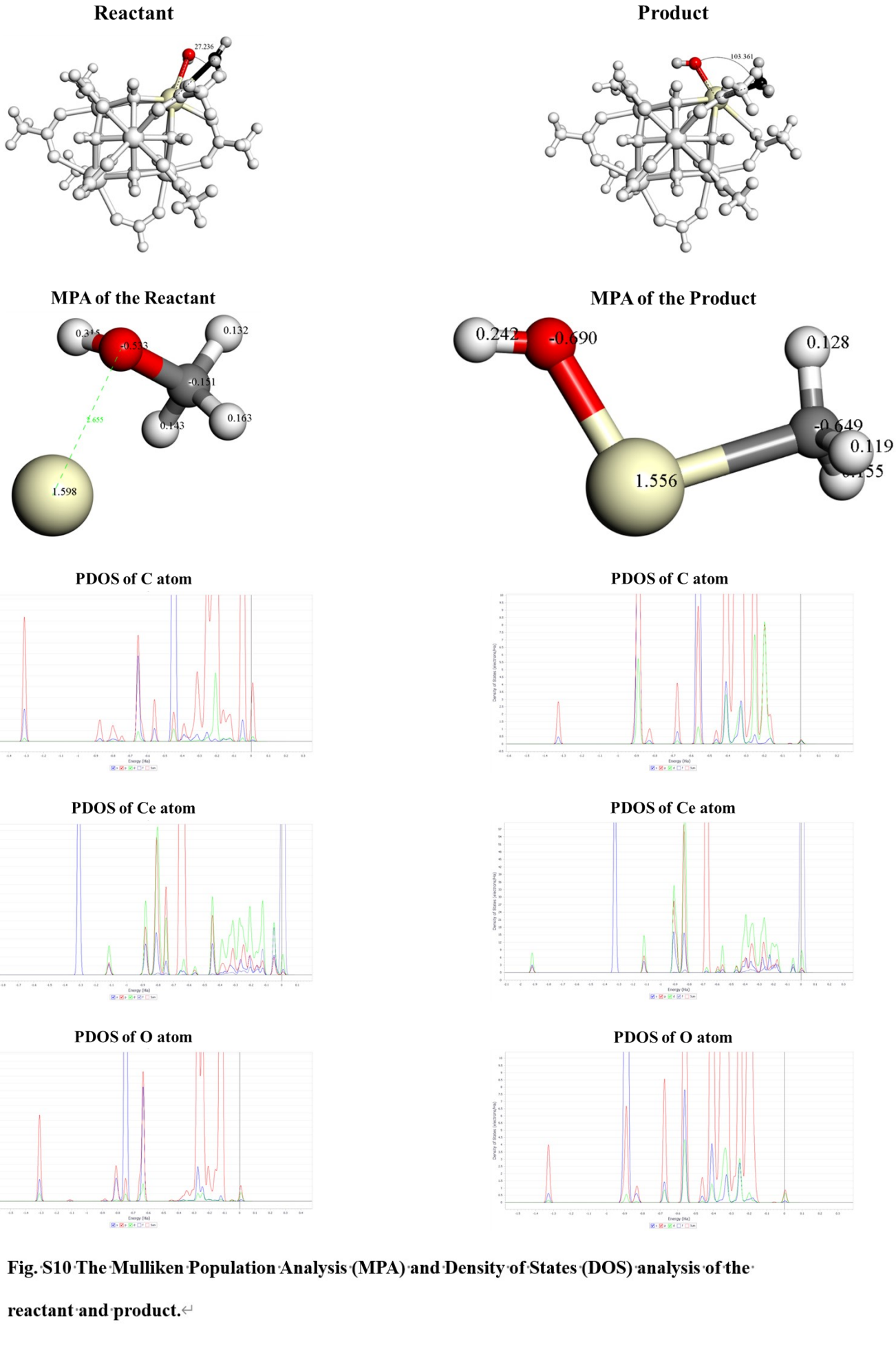

Fig. S10 The Mulliken Population Analysis (MPA) and Density of States (DOS) analysis of the reactant and product.

Section S9 Catalytic conversion of microalgal oil into biodiesel

In this work, biodiesel was prepared by the two-step method. Microalgal lipids were extracted using an optimized Bligh and Dyer protocol (Bligh and Dyer, 1959 [6]). Briefly, 100 mg dried microalgal biomass was fully ground and extracted with a mixture of chloroform (3 mL) and methanol (5 mL). After 3 min of ultrasonic treatment, 5 ml of deionized water was added. Then the chloroform phase containing microalgal lipids was separated by centrifugation (8000r min-1, 3 min), transferred to a glass bottle, and kept at 60 °C for 24 h to evaporate the solvent and obtain microalgal oil.

The obtained microalgal lipids were mixed with methanol (2 ml) and added to 5-ml autoclave. After adding 2wt.% (based on methanol) catalyst, the autoclave was heated to the appropriate temperature and kept at this temperature for 90 minutes. When the reactor was cooled to room temperature, 6 mL *n*-hexane and 4 mL deionized water were added into the mixture to extract biodiesel product. The resulting mixture was centrifuged (8000 r min^{-1}, 3 min) after shaking for 3 min, and the *n*-hexane layer containing biodiesel was separated and transferred to a glass bottle, which was kept in an oven at 60 °C overnight to evaporate the solvent to obtain biodiesel product. The catalyst was separated from the water phase and recovered for the next reaction cycle. The effects of reaction temperature (30-150 °C) and cyclic reaction times on the conversion of the catalyst were investigated.by this method.

The total amount of microalgal lipid that can be converted into fatty acid methyl ester (FAME) was determined by the following method. The lipids were saponified with 4 mL saturated methanolic sodium hydroxide solution at 60 °C for 30 min, and then methanolated with 8 mL methanol containing 5% H_2SO_4 at 90 °C for 60 min. FAME was extracted from the product with *n*-hexane, and the yield and composition of FAME were determined by gas chromatography with a 7890A instrument (Agilent, USA). The lipid content of the microalgae used in this paper was 35.75 wt.%.

Catalytic efficiency was calculated according to：

$$Catalytic\ efficiency = \frac{Amount\ of\ FAME\ produced\ by\ catalyst\ (mg)}{Amount\ of\ total\ lipid\ (mg)}$$

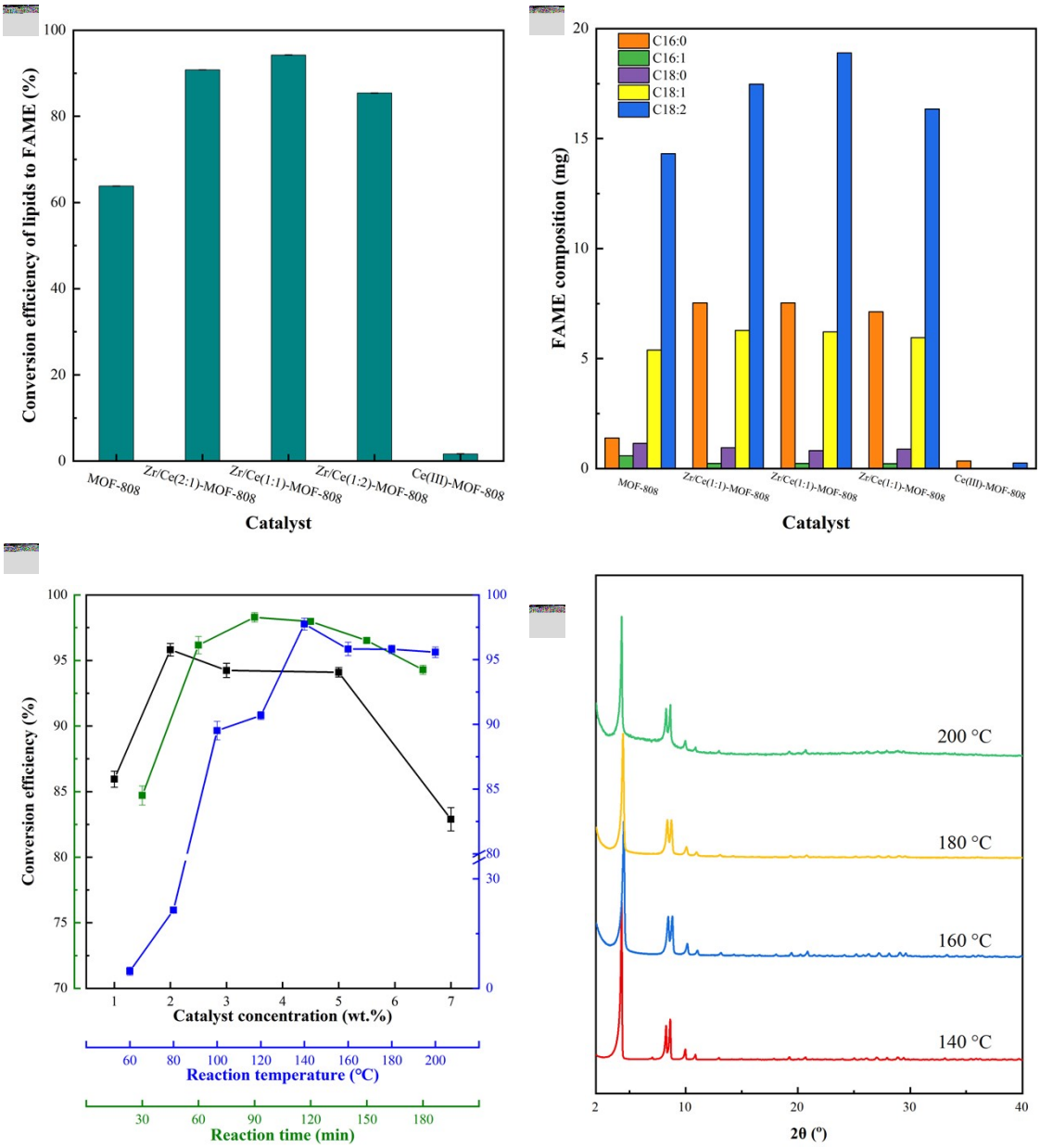

Fig. S11 (a) Conversion efficiency of microalgal lipids to fatty acid methyl ester (FAME) over various catalysts; (b) main compositions of FAME; (c) effects of reaction conditions on conversion effi ciency; (d) XRD analysis of Zr/Ce(1:1)-MOF-808 catalyst post-reaction at a catalyst loading of 2 wt.% and a reaction time of 2 hours.

The reaction to biodiesel was conducted using lipids from 100 mg microalgae and 2 mL methanol as the reaction substrate. The catalytic reaction efficiency of the MOF-808 catalysts at a catalyst addition of 3 wt.% (relative to the mass of methanol) and a reaction temperature of 160 °C is shown in Fig. S11a. MOF-808 and Zr/Ce(2:1, 1:1, 1:2)-MOF-808 with rich pore structures had

superior catalytic efficiencies (63.82%, 90.80%, 94.24%, and 85.41%, respectively), while Ce(III)-MOF-808 was very inefficient (1.67%) due to its different structure. The component analysis of the formed fatty acid methyl esters (FAME) was shown in Fig. S11b and mainly consisted of C16:0, C16:1, C18:0, C18:1, C18:2, and C20:5. Compared to MOF-808, the catalyst Zr/Ce(1:1)-MOF-808 formed a catalytic product mixture with a significant increase in C16:0 and C18:2, indicating enhanced catalytic activity. When using Zr/Ce(1:2)-MOF-808, however, all components in the catalytic product mixture decreased, which echoed the increase in inactive amorphous material.

For the catalyst Zr/Ce(1:1)-MOF-808, we investigated the effect of catalyst addition, reaction temperature, and reaction time on conversion efficiency. The black curve in Fig. S11c reveals that at a temperature of 160 °C and a reaction time of 2 h, the efficiency of the reaction increased and then decreased with increasing catalyst addition. Zr/Ce(1:1)-MOF-808 had a relatively high conversion efficiency (95.82%) at an addition of 2 wt.%. The blue curve in Fig. S11c shows the variation in conversion efficiency with temperature at a catalyst addition of 2 wt.% and a reaction time of 2 h. Zr/Ce(1:1)-MOF-808 demonstrated a relatively high conversion efficiency (97.97%) at reaction temperatures up to 140 °C, which was a relatively low temperature for a solid acid catalyst (the usual optimum temperature for solid acid catalysts is around 200 °C). The Zr/Ce(1:1)-MOF-808 catalyst, which underwent performance tests for temperature-dependent conversion efficiency, was subjected to additional XRD characterizations to investigate its reaction stability. The results, as illustrated in Fig. S11d, reveal negligible alterations in the XRD patterns of the catalyst before and after the reaction, indicating the stability of the catalyst lattice.

The green curve in Fig. S11c represents the conversion efficiency of Zr/Ce(1:1)-MOF-808 with reaction time at a catalyst addition of 2 wt% and a reaction temperature of 140 °C. The highest conversion efficiency of 98.29% was achieved at 90 min, followed by a slight decrease, probably due to the oxidation of partially unsaturated FAME. In addition, thermogravimetric tests revealed that Zr/Ce(1:1)-MOF-808 was thermally stable under the given reaction conditions and extremely insoluble in methanol.

References

1 J. Jiang, F. Gándara, Y.-B. Zhang, K. Na, O. M. Yaghi and W. G. Klemperer, *J. Am. Chem. Soc.*, 2014, **136**, 12844–12847.

2 C. A. Trickett, T. M. O. Popp, J. Su, C. Yan, J. Weisberg, A. Huq, P. Urban, J. Jiang, M. J. Kalmutzki, Q. Liu, J. Baek, M. P. Head-Gordon, G. A. Somorjai, J. A. Reimer and O. M. Yaghi, *Nat. Chem.*, 2019, **11**, 170–176.

3 N. Prasetyo and F. I. Pambudi, *International Journal of Hydrogen Energy*, 2021, **46**, 4222–4228.

4 S. Grimme, J. Antony, S. Ehrlich and H. Krieg, *The Journal of Chemical Physics*, 2010, **132**, 154104.

5 S. Grimme, *Journal of Computational Chemistry*, 2006, **27**, 1787–1799.

6 M. J. Ramalhosa, P. Paiga, S. Morais, M. Rui Alves, C. Delerue-Matos and M. B. Prior Pinto Oliveira, *Food Chem.*, 2012, **131**, 328–336.